applied sciences

MDPI

Article

Efficient Fixed-Switching Modulated Finite Control Set-Model Predictive Control Based on Artificial Neural Networks

Abualkasim Bakeer [1,2], Mohammed Alhasheem [3,*] and Saeed Peyghami [4]

[1] Department of Electrical Engineering, Faculty of Engineering, Aswan University, Aswan 81542, Egypt; abualkasim.bakeer@aswu.edu.eg
[2] Department of Electrical Power Engineering and Mechatronics, Tallinn University of Technology, 19086 Tallinn, Estonia
[3] Department of Electrical and Control, Arab Academy for Science, Technology, and Maritime Transport, Cairo 2033, Egypt
[4] Department of Energy Technology, Aalborg University, 9220 Aalborg, Denmark; sap@energy.aau.dk
* Correspondence: m.a.hasheem@aast.edu; Tel.: +20-1117699989

Abstract: The disadvantage of finite control set-model predictive control (FCS-MPC) is that the switching frequency is variable and relies on the sampling time and operating point. This paper describes how to implement a new algorithm to achieve a fixed-switching frequency functionality for the FCS-MPC. The used approach combines the FCS-MPC with the SVPWM, resulting in the calculation of dwell times and the selection of the best two active vectors for the next sample interval. These dwell times have a significant impact on FCS-MPC performance during transient and steady-state conditions, and their values are determined using various mathematical models. To solve the problem of the fixed-switching frequency with lower harmonics distortion compared to the conventional modulated MPC (M^2PC), an ANN-based trained network is proposed to calculate the duty-cycle of the applied vectors and thus the dwell time in the next sampling interval. The ANN network receives the cost functions of the two active vectors and the zero vector from the M^2PC control algorithm and determines the optimal duty-cycle for each vector based on a proper tuning. In this way, three goals are achieved, the first goal is that the algorithm explicitly obtains a fixed-switching frequency, and secondly, the cost is as simple as the conventional M^2PC. Finally, the feature of including objectives and non-linearity is still applicable. The paper's case study used the two level voltage source inverter (2L-VSI) for uninterruptible power supply (UPS) applications. The results based on MATLAB/Simulink revealed that the ANN-M^2PC has retained all FCS-MPC features in addition to operating at a fixed-switching frequency, while the power quality is significantly enhanced.

Keywords: finite control set-model predictive control (FCS-MPC); space vector pulse width modulation (SVPWM); dwell-time calculations; artificial neural networks (ANN); fixed-switching frequency; total harmonic distortion (THD)

check for updates

Citation: Bakeer, A.; Alhasheem, M.; Peyghami, S. Efficient Fixed-Switching Modulated Finite Control Set-Model Predictive Control Based on Artificial Neural Networks. *Appl. Sci.* **2022**, *12*, 3134. https://doi.org/10.3390/app12063134

Academic Editor: Giovanni Petrone

Received: 5 February 2022
Accepted: 16 March 2022
Published: 18 March 2022

Publisher's Note: MDPI stays neutral with regard to jurisdictional claims in published maps and institutional affiliations.

Copyright: © 2022 by the authors. Licensee MDPI, Basel, Switzerland. This article is an open access article distributed under the terms and conditions of the Creative Commons Attribution (CC BY) license (https://creativecommons.org/licenses/by/4.0/).

1. Introduction

FCS-MPC has several distinguishing characteristics, including quick response, simple concept, ease of constraint inclusion, and nonlinearity [1,2]. However, due to the action of the FCS-MPC, which is delivered straight forward to the converter switches without any modulation stage, it has the disadvantage of variable switching frequency [3]. Several challenges may develop when the converter runs at a variable switching frequency, including circuit resonance, magnetic component and filter complexity, and a lack of power quality for critical applications [4,5].

There are numerous approaches to adjust the frequency and obtain a fixed switching action for converters controlled by the FCS-MPC. The first method is to include an extra term in the cost function that accounts for the converter switches' previous switching patterns [6]. In addition to the fundamental disadvantage of not being able to choose from a restricted number of acceptable switching states due to the lack of a modulator, this method necessitates an additional weighting component, which could make the tuning of cost

function more difficult [7]. Another option is to employ band-stop filters (i.e., notch filters) to regulate the harmonics. This strategy may provide problems with stability, particularly in grid-connected applications [8]. The alternative way is to employ the periodic control technique, which is based on assessing up and down switching events to achieve the modulation behavior [9]. In this procedure, a correctly tuned factor is also required for many operations. Another option is to remove the excess term and use a modulation technique like space vector modulation (SVM) [10]. In this scenario, the FCS-MPC and SVM combination provides a decent performance in terms of fast response and fixed-switching frequency [11]. In this approach, there are numerous ways to compute the dwell times associated with each applied vector. One is based on the traditional SVM, while others use virtual methods to calculate dwell time appropriately [12].

The research community's most recent tendency is to fix the FCS-MPC switching frequency, which is based on the use of modulated MPC [13]. Approaches such as discrete space vector [14], deadbeat predictive control [15,16], and predictive PWM methods result in intricate expressions for switching time calculations [17,18]. Moreover, they are not intuitive, because introducing other objectives into the cost function are difficult during the control design [19,20]. In such methods, the optimal vector is not applied during the whole sampling period, but it is applied in a part of the sampling interval, while in the remaining part, another vector can be applied.

To address these issues, a novel method has been presented that allows operation at a fixed switching frequency, while keeping the benefits of the FCS-MPC controller [21]. This method uses a linear PI controller to simulate the implementation of SVM by using two active vectors and two zero vectors. The time of each vector should be determined and optimized using the same methodology as the conventional SVPWM to reach a certain goal. Dwell times are what they are called, and this is referred to as MMPC or M^{2}PC [21].

On the other hand, the use of artificial neural networks (ANNs)-based approaches in the field of power electronics is rapidly growing. The use of neural networks for dynamical system control was first proposed in the early 1990s [22]. Multi-layer perceptions were used for a variety of tasks, including system identification and control law implementation. ANN-based controllers and estimators, in particular, have been widely employed to identify and operate power converters and motor drives [23]. The advantages of ANN-based controllers include: they can generally improve the performance of the system when properly tuned, and they can be created based on data received from a real system or plant in the lack of expert knowledge. They do, however, necessitate a considerable amount of training data. However, as the current study shows, this is not a significant disadvantage because trustworthy modeling techniques may be used to acquire data [24,25].

In much prior research, the ANN has been used to replace the predictive controller, which considers the converter as a black box. The main disadvantage of this strategy is that it is limited in terms of flexibility because of the inability to add further constraints to the objective function once the ANN network has been established [26,27]. This leads to the loss of one of the characteristics of the MPC, which is the potential to deal with several constraints, within a single control law. On the other hand, other studies have employed the ANN to fine-tune several targets in order to obtain reduced THD [28].

The objective of this paper is to apply ANN to optimally define the duty-cycle and thus the dwell time associated with the M^{2}PC method in an accurate way. The technique can reserve the converter operation at a fixed-switching frequency, while the THD improves greatly, and the M^{2}PC's properties are preserved. The conventional M^{2}PC for the 2L-VSI will be discussed in Section 2, while the proposed ANN-M^{2}PC will be discussed in Section 3. The simulation results and discussion are given in Section 4, while the conclusion is reported in Section 5.

2. Conventional FCS-MPC for the 3-Phase 2L-VSI Based on SVPWM

Many applications have been proposed for MPC, including electrical drivers, UPS, and grid-connected inverters [6]. FCS-MPC is based on the premise of employing a discrete model of the power converter with its associated filter to anticipate the future behavior of all potential control inputs, and then applying the best one that minimizes a predetermined cost function (CF) at each sampling time (T_s). The main concept is to harness the microcon-

troller's raw processing capability to incorporate all control loops into a single algorithm that takes into account the converter's model and the accompanying filter.

The general block diagram of FCS-MPC to control a three-phase voltage source inverter with an *LC* filter in the output is shown in Figure 1. The FCS-MPC procedure is conducted sequentially in its most basic version, and at the start of each sampling time, it applies a new switching pattern that is determined from the previous step. It then receives new and updated measurements in order to select a new switching pattern. The three-phase 2L-VSI power circuit is considered, with the two switches in each leg operating in a complementary mode to avoid short-circuit across the input source. The switching states are represented by S_a, S_b, and S_c switching signals, which are specified as follows:

$$S_a = \begin{cases} 1 \text{ if } S_1 \text{ on and } S_4 \text{ off} \\ 0 \text{ if } S_1 \text{ off and } S_4 \text{ on} \end{cases} \quad (1)$$

$$S_b = \begin{cases} 1 \text{ if } S_2 \text{ on and } S_5 \text{ off} \\ 0 \text{ if } S_2 \text{ off and } S_5 \text{ on} \end{cases} \quad (2)$$

$$S_c = \begin{cases} 1 \text{ if } S_3 \text{ on and } S_6 \text{ off} \\ 0 \text{ if } S_3 \text{ off and } S_6 \text{ on} \end{cases} \quad (3)$$

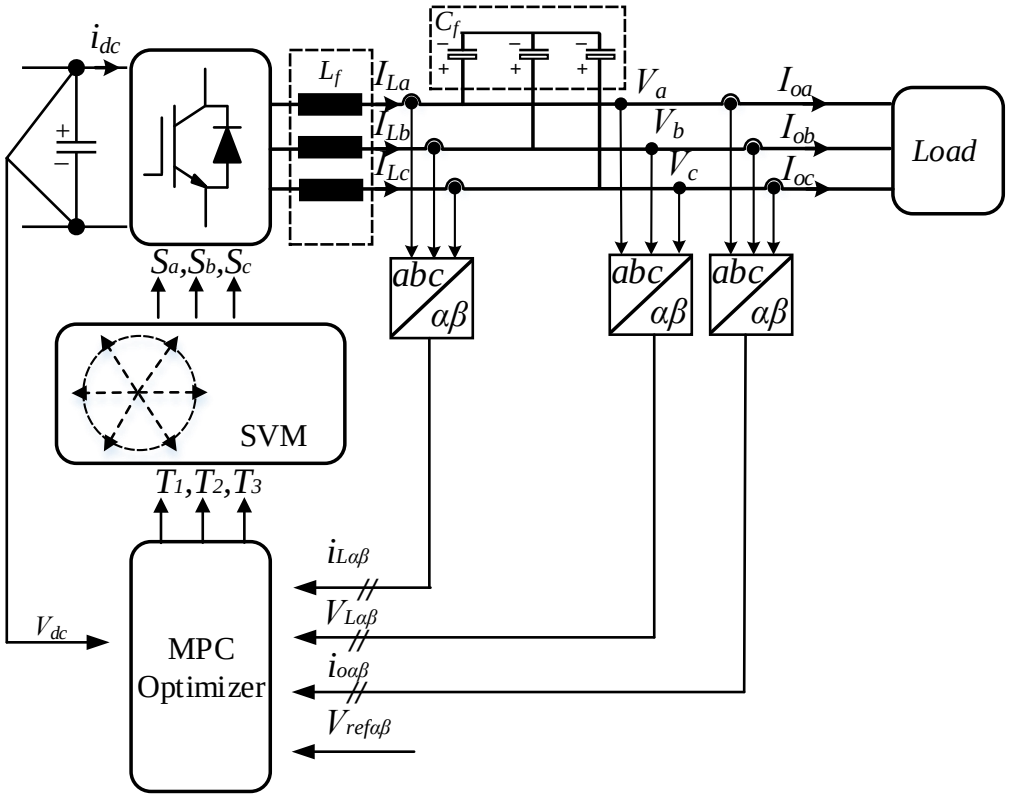

Figure 1. Schematic of the 2L-VSI for UPS applications based on M^{2}PC.

The voltage across filter inductance (L_{fa}, L_{fb}, L_{fc}) can be written in a vectorial form as:

$$L_f \frac{\mathrm{d}I_{L_f}}{\mathrm{d}t} = V_i - V_{C_f} \quad (4)$$

where L_f is the filter inductance, I_{L_f} is the filter current, and V_{C_f} is the filter voltage, and V_i denotes the system's inverter voltage, which has eight different voltage vectors (i.e., six active vectors and two zero vectors), as illustrated in Figure 2. It is clear that the space

vector diagram has six sectors. Mathematically, the equation that defines the dynamic behavior of the output voltage is as follows:

$$C_f \frac{dV_{C_f}}{dt} = I_{L_f} - I_o \tag{5}$$

where I_o is the load current, which can be measured or estimated, and C_f is the filter capacitance (C_{fa}, C_{fb}, C_{fc}). In the state space model, these equations can be expressed as:

$$\frac{dX}{dt} = AX + B_1 V_i + B_2 I_o \tag{6}$$

where

$$X = \begin{bmatrix} I_{L_f} \\ V_{c_f} \end{bmatrix} \tag{7}$$

$$A = \begin{bmatrix} -R/L_f & -1/L_f \\ 1/C_f & 0 \end{bmatrix} \tag{8}$$

$$B_1 = \begin{bmatrix} 1/L_f \\ 0 \end{bmatrix} \tag{9}$$

$$B_2 = \begin{bmatrix} 0 \\ -1/C_f \end{bmatrix} \tag{10}$$

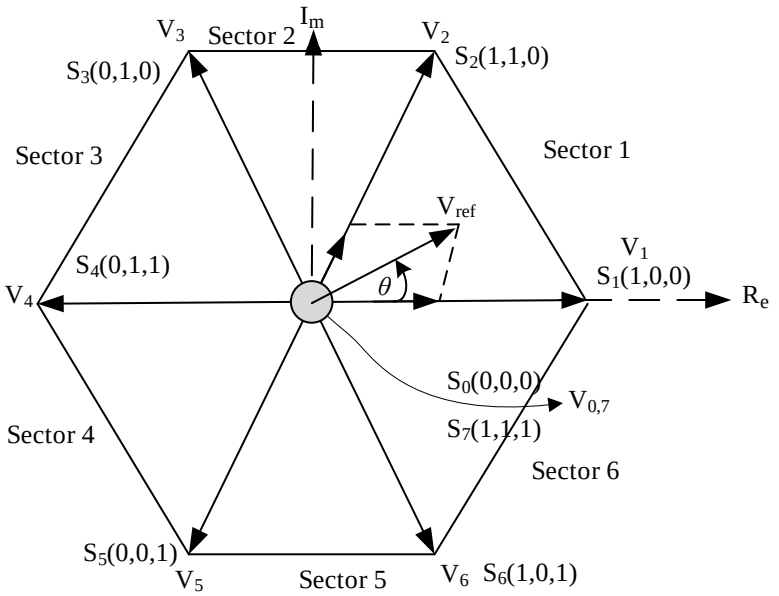

Figure 2. Space vector diagram and the voltage vectors generated by the inverter (V_i).

A discrete model is obtained from (6) and it can be expressed as follows:

$$x(k+1) = A_q x(k) + B_q V_i(k) + B_{dq} I_o(k) \tag{11}$$

where

$$A_q = exp^{AT_s} \tag{12}$$

$$B_q = \int_0^{T_s} exp^{A\tau} B_1 d\tau \tag{13}$$

$$B_{dq} = \int_0^{T_s} exp^{A\tau} B_2 d\tau. \tag{14}$$

This model is used to predict the filter current in L_f and voltage across C_f for any input voltage and different loading conditions. The evaluation of cost function influences

the choice of the optimal output voltage vector to be applied in the next sampling interval. For such a system, the main control target is to fix the inverter output voltage, therefore the CF will be defined as follows:

$$J = (V^*_{C_{f\alpha}} - V_{C_{f\alpha}}(k+1))^2 + (V^*_{C_{f\beta}} - V_{C_{f\beta}}(k+1))^2 \tag{15}$$

where $V^*_{C_f\alpha}$ and $V^*_{C_f\beta}$ are the real and imaginary parts of the reference voltage, respectively.

In space vector modulation, it is possible to define each available vector in the 2L-VSI in ($\alpha\beta$) plane, as shown in Figure 2. The modulated MPC technique calculates the prediction of the two active vectors that compose each sector at every sampling time. The cost function, defined by (15), is evaluated for each sector. Each prediction is evaluated based on (11), where the duty-cycle for the two active vectors (d_i) are calculated by solving the following equation:

$$d_i = \frac{\delta}{J_i} \tag{16}$$

where δ is the constant of proportionality, the subscript i denotes the adjacent vectors, in this case (i = 1; 2) and i = 0 corresponds to the duty-cycle of a zero vector, which is evaluated only one time, and J_i is equivalent cost function that the sum of product of all possible two cost function combination from the three vectors cost functions. The sum of the duty-cycle associated with the two active vectors and zero vector equals to unity as:

$$d_1 + d_2 + d_0 = 1 \tag{17}$$

By solving the previous equations, it is possible to obtain the duty-cycle for each vector as:

$$d_1 = \frac{J_2 J_0}{J_1 J_0 + J_1 J_2 + J_2 J_0} \tag{18}$$

$$d_2 = \frac{J_1 J_0}{J_1 J_0 + J_1 J_2 + J_2 J_0} \tag{19}$$

$$d_0 = \frac{J_1 J_2}{J_1 J_0 + J_1 J_2 + J_2 J_0} \tag{20}$$

Considering these expressions, the new cost function that is evaluated at every T_s for the sector selection, can be defined as:

$$g = d_1 J_1 + d_2 J_2 \tag{21}$$

The two vectors that minimize the CF are selected and applied to the 2L-VSI in the next sampling interval beside the zero vector. After selecting the optimal two vectors and calculating the corresponding duty-cycle, the dwell time associated with each vector can be calculated as in (22). The complete algorithm of M^{2}PC will be executed sequentially as given in Algorithm 1.

$$\begin{aligned} T_1 &= d_1 T_s \\ T_2 &= d_2 T_s \\ T_0 &= d_0 T_s \end{aligned} \tag{22}$$

The conventional MPC control strategy is carried out in the following order: (1) Measuring of MPC input variables; (2) Predicting the output voltage and for the next sample period; (3) Calculating the cost function; (4) Choosing the switching signals that minimize the cost function; (5) Applying the optimized corresponding signals.

In reality, taking into consideration the computation time and applying the selected switching state after the next sample instant is a simple way to compensate for the expected delay. As a result, the control algorithm is updated in the following way: (1) Variables are measured. (2) Application of the switching state (calculated in the previous interval). (3) Estimation of the voltage values at time $t_k + 1$, taking into account the switched state. (4) For all conceivable switching states, prediction of load voltages for the following sampling

instant ($t_k + 2$). (5) For each prediction, the cost function is evaluated. (6) The switching state that minimizes the cost function is chosen. It can be assumed that $V^*_{C_f}(k+1) = V^*_{C_f}(k)$ for the predictive voltage control example, and the cost function can be rewritten as in (15). This approximation will lead to a one-sample delay in the reference tracking of the reference currents. If compensation of the calculation time delay is considered, the reference $V^*_{C_f}(k+2)$ is required. Using the same idea, the future reference can be assumed to be $V^*_{C_f}(k+2) = V^*_{C_f}(k)$, resulting in the following cost function

$$J = (V^*_{C_f\alpha} - V_{C_f\alpha}(k+2))^2 + (V^*_{C_f\beta} - V_{C_f\beta}(k+2))^2. \tag{23}$$

Algorithm 1: Pseudocode of the conventional M^{2}PC with the studied 2L-VSI.

```
Measure I_f(k), I_o(k), V_c(k);
Set g_opt = ∞;
Predict V_0(k+1) at the zero vector;
Calculate J_0 using (15);
for i = 1 : 6 do
    Predict V_1(k+1) using V_i = S(i)V_dc;
    if i < 6 then
        Predict V_2(k+1) using V_i = S(i+1)V_dc;
    else
        Predict V_2(k+1) using V_i = S(1)V_dc;
    Calculate J_1 and J_2 using (15);
    Calculate d_1(i), d_2(i), d_0(i) using (18)–(20);
    Evaluate g(i) = d_1(i)J_1 + d_2(i)J_2;
    if g(i) < g_opt then
        Set g_opt = g(i);
        Set d_1 = d_1(i);
        Set d_2 = d_2(i);
        Set d_0 = d_0(i);
        Set S_n = i;
Calculate dwell times T_1, T_2, T_0 using (22);
```

3. Proposed M^{2}PC Based-ANN for the 2L-VSI

3.1. Motivation of Using ANN in the Proposed System

The artificial neural network (ANN) can be used to model complicated systems in order to save time and effort while analyzing difficult mathematical relationships. It can map nonlinear relation between the input and output using a historical data [29]. The neuron is the fundamental unit of the neural network, as shown in Figure 3, and ANN attempts to imitate the human brain. During the training phase, the neural network attempts to map the relationship between the input and output data by changing the weighting and biasing factors, which are usually initialized randomly, by optimizing the employed cost function. By taking advantage of the flexibility of M^{2}PC at training phase, this work proposes a radial bias function (RBF) ANN-based controller for a three-phase 2L-VSI with an output *LC* filter targeting UPS applications. The goal is getting lower THD and good performance in the output voltage at different types of loads. The proposed controller undergoes two main steps: (i) we use it to evaluate the single objective cost function, as an expert or a teacher for generating the data required for training, validation, and testing phases in an off-line mode, where the proposed neural network applies standard supervised learning under the full-state observation of the system; (ii) when the off-line training is performed, the trained RBF-ANN can successfully calculate the duty-cycle of the two active vectors, which will be applied in the next sampling interval, and then control the output voltage of the inverter as illustrated in Figure 4. We study a performance

comparison between the proposed ANN-M^{2}PC based approach and the conventional MPC, under various operating conditions.

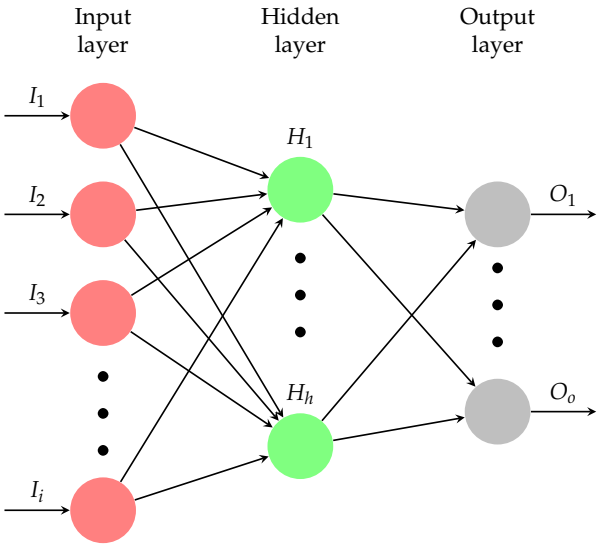

Figure 3. General overview of the ANN structure comprising different layers.

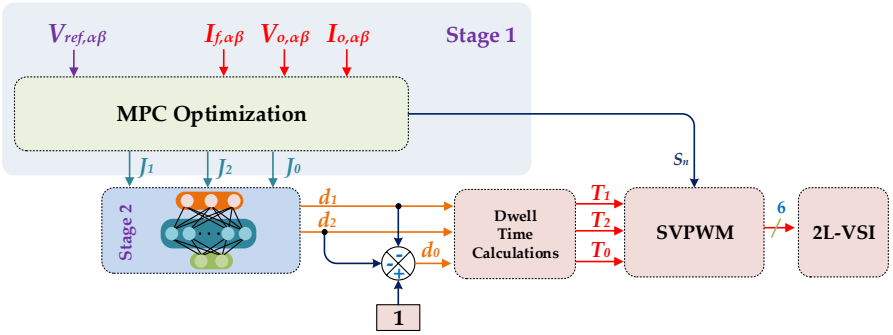

Figure 4. Proposed M^{2}PC based on the ANN to estimate the duty-cycle of each vector in the next sampling period.

3.2. Description of the Implemented ANN Network

In this work, the implemented ANN network is the radial bias function, which has a structure of three layers as one input layer, one hidden layer, and one output layer. The RBF-ANN has simple design, immunity to input noise, and good generalization. These properties allow it to be used for designing flexible control systems.The RBF is utilized as an approximation function to define the active vectors' duty-cycle, and therefore the zero vector duty-cycle can be calculated as well. As shown in Figure 4, the input layer gets the cost function for both active vectors that make up the optimum sector, as well as the cost function for the zero vector. These input features are generated from the conventional algorithm of the modulated MPC at every sampling time. The input layer distributes the network inputs into the next hidden layer. The neurons in the hidden layer, that is, x_i are characterized by the Gaussian nonlinear function as in (24).

$$b_j(x_i) = exp\left(- \frac{\| x_i - \mu_j \|}{2\sigma_j^2} \right) \quad for \;\; j = 1, 2, \ldots, q \tag{24}$$

where q is the number of neurons in the hidden layer, and μ_j, σ_i, and b_j are the centroid, spread width, and the response of the jth hidden neuron, respectively. The output layer combines Gaussian functions, which are weighted by weighting factors for each activation function for neurons, as in (25).

$$Y = \sum_{j=1}^{q} W_j b_j(x_i) \tag{25}$$

where Y is the output of the RBF-ANN, $b_j(x_i)$ is the output of the jth neuron in the hidden layer, and W_j is the weight between the jth neuron in the hidden layer and the node in the output layer.

The dataset for RBF-ANN is selected randomly from different simulation scenarios. Different uncertainties in the following parameters are considered to collect the dataset: filter inductance and capacitance, load impedance, reference output voltage, and sampling interval as listed in Table 1. The total number of raw datasets equals 5000 raws. To ensure that neuron bases may respond to overlapping regions in a search area, the design for each neuron's propagation (σ_i) should have a high value, keeping in mind that the threshold for neurons to react in an equal manner is not too high [30]. In the current case study, it is selected at 25, and the target goal of the RBF-ANN objective function has been achieved after 16 epochs, as shown in Figure 5.

Table 1. Description of training scenarios used for training the proposed RBF-ANN.

Scenario	L_f [mH]	C_f [µF]	R [Ω]	L [mH]	T_s [µs]
1	1	40	10	1	40
2	1	55	11	2	40
3	0.85	50	15	3	60
4	0.50	55	10	4	35
5	0.75	35	12	5	40
6	0.90	45	25	6	50
7	1	40	10	10	50

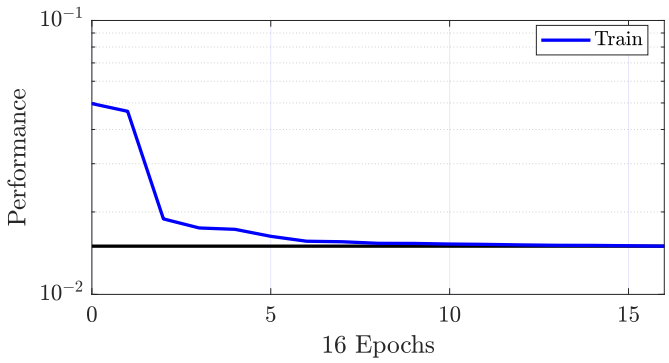

Figure 5. Performance of the utilized RBF-ANN during the training phase.

Following the well training phase of the RBF-ANN network, the testing phase will begin to assess the trained network's effectiveness on unknown data before merging it into the online Simulink model. The performance of the RBF-ANN network during testing with random (i.e., unseen) data is shown in Figure 6. The trained RBF-ANN will be incorporated into the FCS-MPC as shown in the flowchart in Figure 7. It is important to mention that when the sixth sector is being evaluated (i.e., $i = 6$), the voltage of the second vector in this sector should be computed as the first vector (i.e., similar to lines 7–10 in Algorithm 1).

In addition, it is worth noting that when the sector of the optimal two active vectors is odd (that is, 1, 3, or 5), the switching pattern in Figure 8a should be applied to keep the switching frequency constant for one sample period. When the selected sector is even (that is, 2, 4, or 6), the switching pattern in Figure 8b should be used to establish the switching frequency. In this way, the commutation of the 2L-VSI switches will be fixed within a single sampling interval, and thus the fixed-switching operation can be achieved. Additionally, the RBF-ANN network is updated at every sampling interval with the new cost function of the active vectors and zero vector. Based on these values, new duty-cycle values will be

given by the RBF-ANN output, and therefore the dwell time can be recalculated to make the converter output voltage close to its reference as possible.

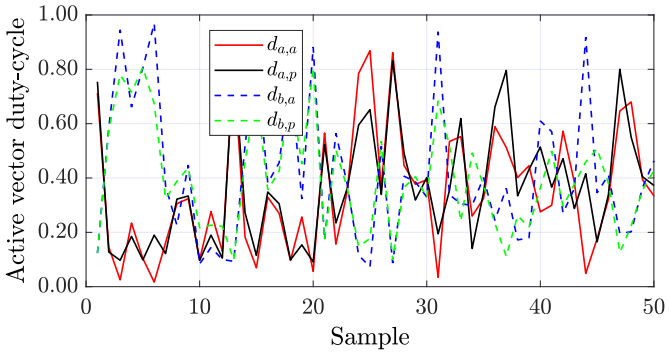

Figure 6. Performance of the utilized RBF-ANN during the testing phase.

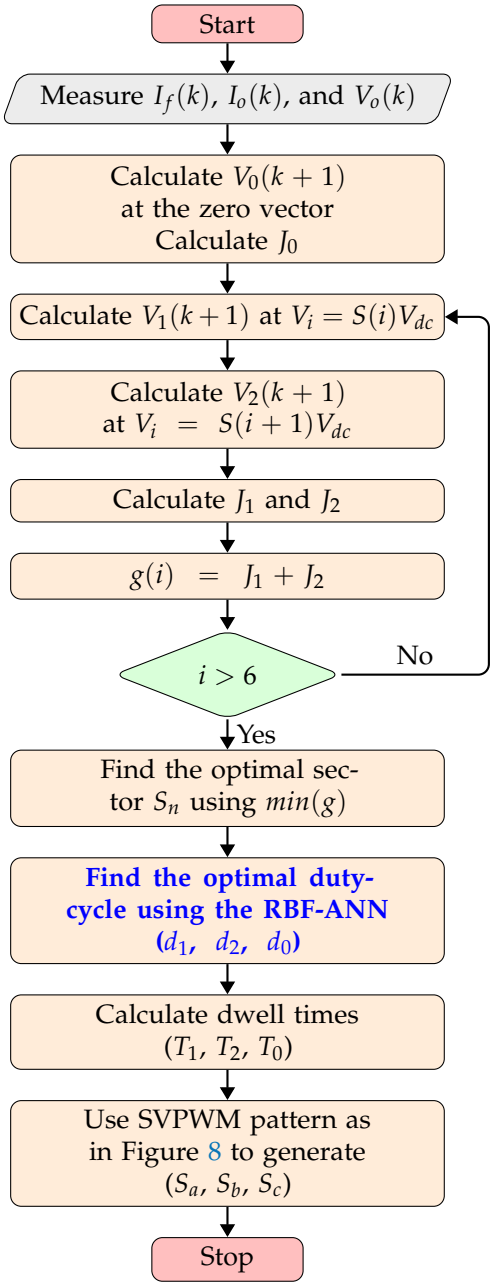

Figure 7. Flowchart of the proposed M^{2}PC based on the RBF-ANN for the 2L-VSI.

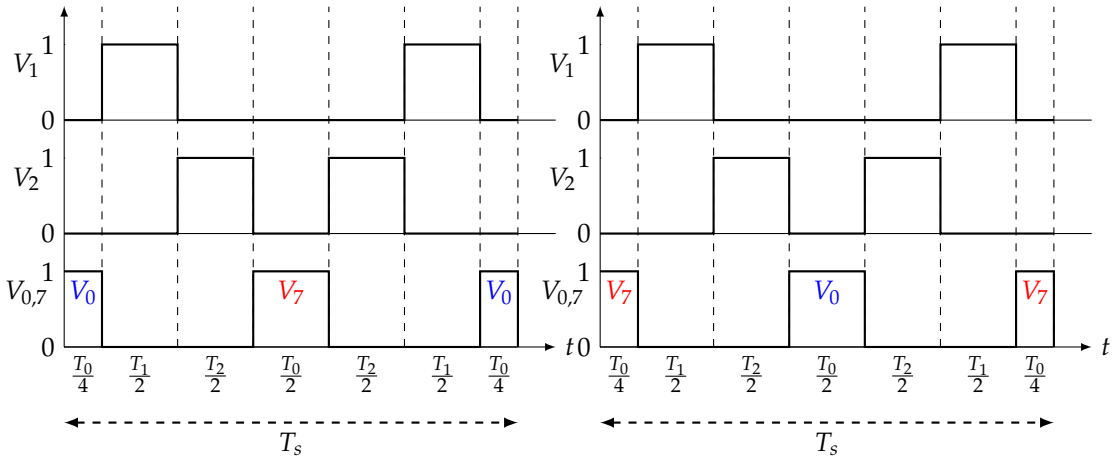

Figure 8. Switching pattern of the applied vectors when the optimal sector is: (**a**) odd, (**b**) even.

4. Simulation Results and Discussion

In this section, we will show the performance of the 2L-VSI using the conventional M^{2}PC and the proposed ANN-M^{2}PC. To assess its performance, it is of paramount importance to check several system behaviors feeding both linear and nonlinear loads. The steady-state behavior, transient response performance, harmonic spectrum, and the total harmonic distortion of both control schemes will be investigated as well. Table 2 summarizes the system parameters, which were used for both control strategies, while Figure 9 shows the simulink modeling for the simulation results.

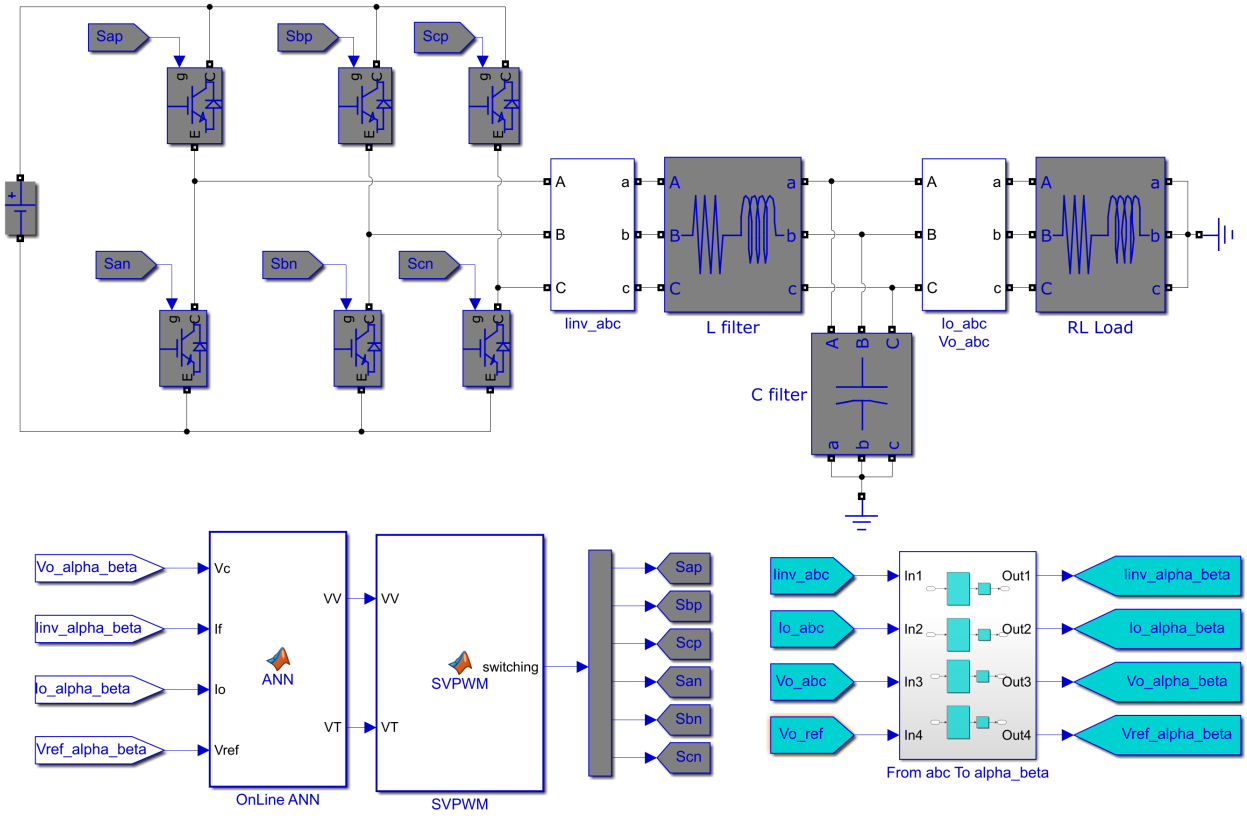

Figure 9. Simulink model for the proposed ANN-M^{2}PC.

Table 2. Parameters of the studied 2L-VSI.

Parameter	Symbol	Value
Input voltage	V_{dc}	700 V
Filter inductance	L_f	2 mH
Filter capacitance	C_f	50 µF
Switching frequency	F_{sw}	10 kHz
Sampling time	T_s	100 µs
Nominal RMS output voltage (L-L)	$V_{o,ref}$	380 V

Figure 10 shows the converter output voltage (V_{o,α_β}) controlled by the M^{2}PC and the proposed ANN-M^{2}PC feeding a linear *RL* load. Both controllers are following a voltage reference as the only objective of their cost function. In addition, the load current is shown in Figure 11. It gives an insight on the performance of the 2L-VSI using the ANN-M^{2}PC compared to M^{2}PC during the instant of load change at 0.1 s. That gives a fair comparison as the available opportunity is equal for both controllers by tracking only the voltage at every sampling time based on the CF definition as in (23), but with different approaches for dwell-time calculations. It has been detected that the error from the reference of the conventional tracking algorithm is high. The error at some points in time can be spiky, resulting in a risk of stability issues based on the intended application. This outcome is verified when the error difference is calculated for both the conventional and proposed algorithms, as shown in Figure 12.

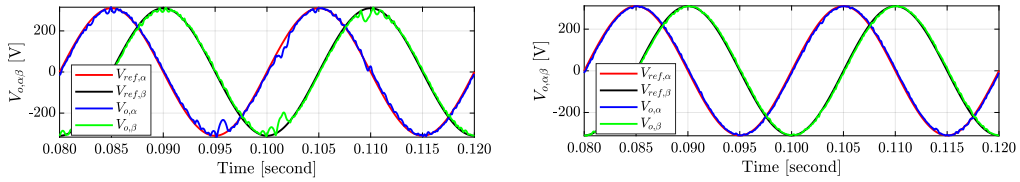

(**a**) (**b**)

Figure 10. Dynamic performance of the output voltage in both control algorithms when the load is stepped-up at 0.1 s: (**a**) conventional M^{2}PC, (**b**) proposed ANN-M^{2}PC.

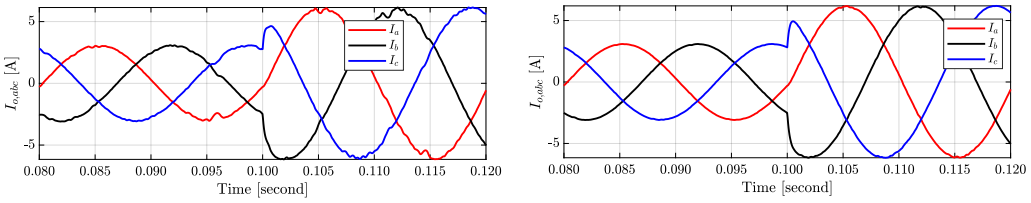

(**a**) (**b**)

Figure 11. Dynamic performance of the load current in both control algorithms when the load is stepped-up at 0.1 s: (**a**) conventional M^{2}PC, (**b**) proposed ANN-M^{2}PC.

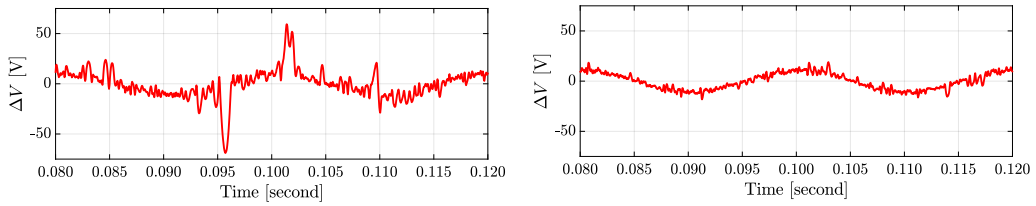

(**a**) (**b**)

Figure 12. Tracking error of the phase voltage: (**a**) conventional M^{2}PC, (**b**) proposed ANN-M^{2}PC.

Using the proposed algorithm leads to a better power quality compared to the conventional M^{2}PC. In addition, two important aspects have been retained by using the proposed

algorithm, firstly, the algorithm can still accept adding more constraints into its operating cost function. Another aspect is that the fast response and the fixed-switching frequency are achieved, while the power quality is significantly enhanced. This is illustrated in Figure 13 by calculating the THD for both conventional and proposed algorithms at different sampling times. It is clear that the proposed approach has a superior performance compared to the conventional M^{2}PC, as it has lower THD by around 50% in all the tested sampling intervals.

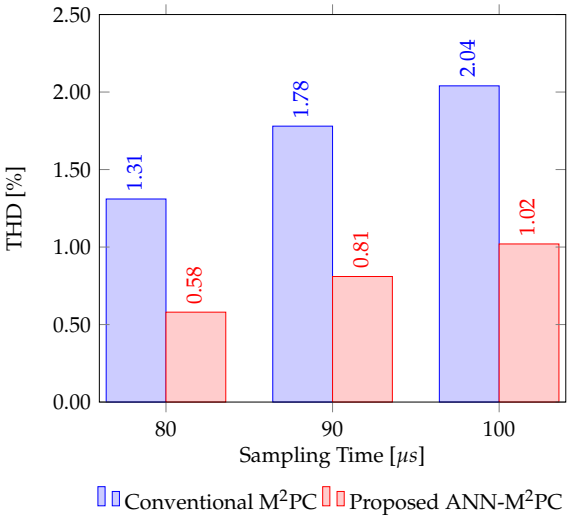

Figure 13. Comparison of total harmonic distortion at different sampling times.

Moreover, Figures 14 and 15 show how the output voltage and current at the same ground of truth have incredibly enhanced and give better shape, respectively. That is a direct result of achieving an optimal switching state, as shown in Figure 16. As it may be noticed that in the proposed ANN-M^{2}PC, the algorithm always keeps the sector selection in a certain time span repetitive and that behavior will introduce better quality compared to the conventional M^{2}PC.

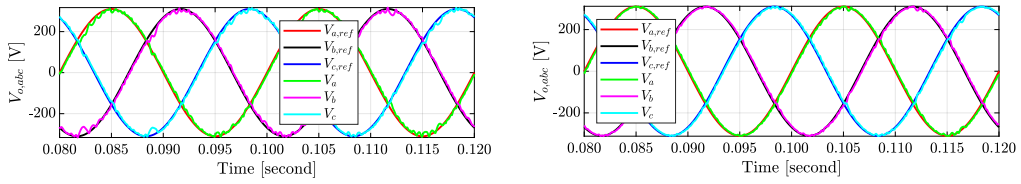

(**a**) (**b**)

Figure 14. Voltage reference tracking performance during the steady-state operation with non-linear load using: (**a**) conventional M^{2}PC, (**b**) proposed ANN-M^{2}PC.

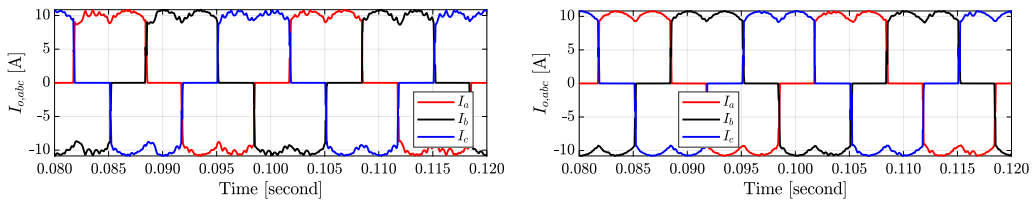

(**a**) (**b**)

Figure 15. Current of non-linear load at steady-state operation: (**a**) conventional M^{2}PC, (**b**) proposed ANN-M^{2}PC.

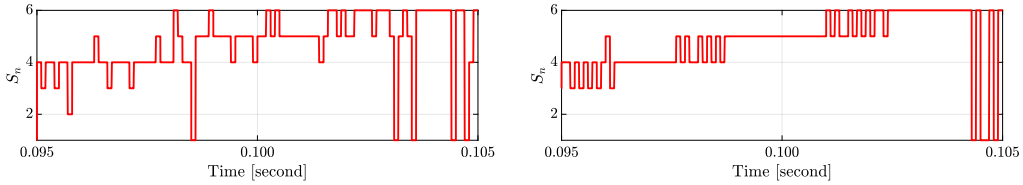

(**a**) (**b**)

Figure 16. Optimal switching sector for the 2L-VSI: (**a**) conventional M^{2}PC, (**b**) proposed ANN-M^{2}PC.

Figure 17 highlights the switching frequency characteristics, which shows a fixed-switching operation at 10 kHz. It can be noticed that the low order harmonics in the conventional M^{2}PC cause a high THD while, in the same zone, the proposed ANN-M^{2}PC has lower harmonics distortion and thus avoid resonance issues.

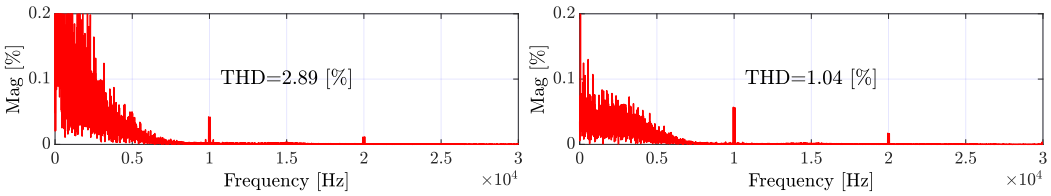

(**a**) (**b**)

Figure 17. FFT spectrum for the phase voltage: (**a**) conventional M^{2}PC, (**b**) proposed ANN-M^{2}PC.

Over and above, the controller is operating at a sampling time of 100 µs, and the execution time with the conventional M^{2}PC is calculated as 6.24 µs, while with the proposed ANN-M^{2}PC is 9.87 µs. It is clear that the computation burden is slightly higher at the same ground truth of the converter parameters and the operating point. The algorithm is running on a personal computer employing an Intel© Core™ i5-8265U processor operating at 1.60 GHz and 16 GB of RAM.

On the other hand, the robustness of the controller at different mismatch conditions is an essential aspect. Therefore, a couple of tests, as an example, have been conducted to assess the performance of the ANN-M^{2}PC under the mismatch of filter inductance or capacitance. It can be clearly seen from Figures 18 and 19 that there is a significant enhancement in the controller robustness compared to the conventional M^{2}PC.

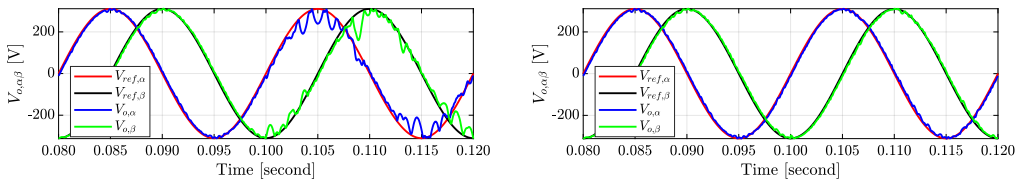

(**a**) (**b**)

Figure 18. L_f mismatch test for both control algorithms (i.e., after the instant 0.1 s, L_f is reduced by 10% of its initial value): (**a**) conventional M^{2}PC, (**b**) proposed ANN-M^{2}PC.

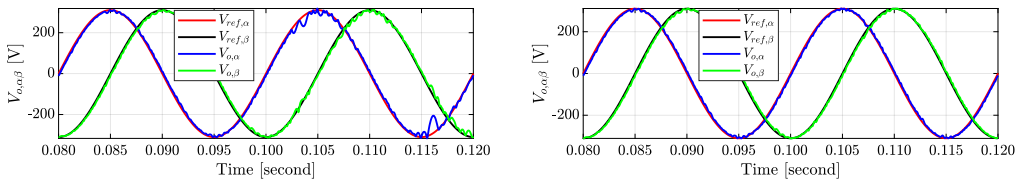

(**a**) (**b**)

Figure 19. C_f mismatch test for both control algorithms (i.e., after the instant 0.1 s, C_f is reduced by 10% of its initial value): (**a**) conventional M^{2}PC, (**b**) proposed ANN-M^{2}PC.

Finally, Figure 20 validates that the proposed ANN-M^{2}PC determines the duty-cycle optimally rather than with unnecessary magnitudes as obtained from the conventional M^{2}PC. In addition, the optimal duty-cycle can be obtained by correctly training the ANN network based on accurate and diverse dataset. The benefit of the proposed system is that the FCS-MPC algorithm for UPS applications does not need to add additional terms into the cost function to improve the power quality and therefore increase the frequency of switching to higher levels. This means that the proposed idea in this paper can be applied as an explicit FCS-MPC without the need to add the voltage tracking and its derivative into the cost function to enhance the power quality.

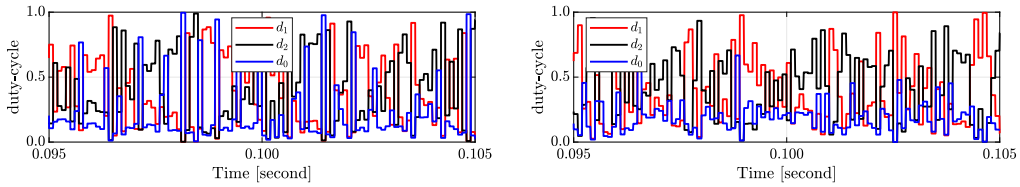

Figure 20. Duty-cycle for the two active vectors and zero vector with: (**a**) conventional M^{2}PC, (**b**) proposed ANN-M^{2}PC.

5. Conclusions

In this paper, an ANN-M^{2}PC control technique based on the radial bias function is proposed for a voltage source inverter with an output *LC* filter for UPS applications. This allows the control system to improve the voltage tracking performance for both linear and nonlinear loads, resulting in low THD. The proposed technique retains all model predictive control and space vector properties, and allows a fixed-switching frequency operation. It is worth noting that the cost function has only one goal and no tunable variables. As a result, the proposed controller can provide optimum performance over a wide range of operations. In this way, the system's steady-state and transient performance is comparable to that of a traditional M^{2}PC, but with significantly better power quality and a little increase in computational burden.

Author Contributions: Conceptualization, A.B.; methodology, A.B. and M.A.; software, A.B.; validation, A.B. and M.A.; formal analysis, A.B. and M.A.; investigation, A.B. and M.A.; resources, A.B.; data curation, A.B.; writing—original draft preparation, A.B. and M.A.; writing—review and editing, all authors; visualization, A.B. and M.A.; supervision, all authors; project administration, S.P.; funding acquisition, S.P. All authors have read and agreed to the published version of the manuscript.

Funding: This research received no external funding.

Institutional Review Board Statement: Not applicable.

Informed Consent Statement: Not applicable.

Data Availability Statement: Not applicable.

Conflicts of Interest: The authors declare no conflict of interest.

References

1. Carrasco, J.M.; Franquelo, L.G.; Bialasiewicz, J.T.; Galván, E.; PortilloGuisado, R.C.; Prats, M.M.; León, J.I.; Moreno-Alfonso, N. Power-electronic systems for the grid integration of renewable energy sources: A survey. *IEEE Trans. Ind. Electron.* **2006**, *53*, 1002–1016. [CrossRef]
2. Geldenhuys, J.M.; du Toit Mouton, H.; Rix, A.; Geyer, T. Model predictive current control of a grid connected converter with LCL-filter. In Proceedings of the 2016 IEEE 17th Workshop on Control and Modeling for Power Electronics (COMPEL), Trondheim, Norway, 27–30 June 2016; pp. 1–6. [CrossRef]
3. Mohamed, I.S.; Zaid, S.A.; Abu-Elyazeed, M.F.; Elsayed, H.M. Classical methods and model predictive control of three-phase inverter with output LC filter for UPS applications. In Proceedings of the 2013 International Conference on Control, Decision and Information Technologies (CoDIT), Hammamet, Tunisia, 6–8 May 2013; pp. 483–488.
4. Rodriguez, J.; Cortes, P. *Predictive Control of Power Converters and Electrical Drives*, 1st ed.; John Wiley & Sons: Hoboken, NJ, USA, 2012; Volume 40, Chapter 5, p. 181.

5. Nauman, M.; Hasan, A. Efficient implicit model-predictive control of a three-phase inverter with an output LC filter. *IEEE Trans. Power Electron.* **2016**, *31*, 6075–6078. [CrossRef]
6. Vazquez, S.; Rodriguez, J.; Rivera, M.; Franquelo, L.G.; Norambuena, M. Model predictive control for power converters and drives: Advances and trends. *IEEE Trans. Ind. Electron.* **2017**, *64*, 935–947. [CrossRef]
7. Cortés, P.; Ortiz, G.; Yuz, J.I.; Rodríguez, J.; Vazquez, S.; Franquelo, L.G. Model predictive control of an inverter with output LC filter for UPS applications. *IEEE Trans. Ind. Electron.* **2009**, *56*, 1875–1883. [CrossRef]
8. Alhasheem, M. Improvement of Transient Power Sharing Performance in Parallel Converter System and Microgrids. Ph.D. Thesis, Faculty of Engineering and Science, Aalborg University, Aalborg, Denmark, 2019; 91p, ISSN 2446-1636.
9. Aguirre, M.; Kouro, S.; Rojas, C.A.; Rodriguez, J.; Leon, J.I. Switching frequency regulation for fcs-mpc based on a period control approach. *IEEE Trans. Ind. Electron.* **2018**, *65*, 5764–5773. [CrossRef]
10. Zhang, Y.; Liu, J.; Fan, S. On the inherent relationship between finite control set model predictive control and SVM-based deadbeat control for power converters. In Proceedings of the IEEE Energy Conversion Congress and Exposition (ECCE), Cincinnati, OH, USA, 1–5 October 2017; pp. 4628–4633. [CrossRef]
11. Riveros, J.A.; Rivera, M.; Rodriguez, C.; Galea, M.; Buticchi, G.; Wheeler, P. Predictive Torque Control with Fixed Switching Frequency for Induction Motor Drives. In Proceedings of the IEEE International Conference on Industrial Technology (ICIT), Buenos Aires, Argentina, 26–28 February 2020; pp. 211–216. [CrossRef]
12. Jiang, C.; Du, G.; Du, F.; Lei, Y. A Fast Model Predictive Control with Fixed Switching Frequency Based on Virtual Space Vector for Three-Phase Inverters. In Proceedings of the IEEE International Power Electronics and Application Conference and Exposition (PEAC), Shenzhen, China, 4–7 November 2018; pp. 1–7. [CrossRef]
13. Rojas, F.; Kennel, R.; Cardenas, R.; Repenning, R.; Clare, J.C.; Diaz, M. A new space-vector-modulation algorithm for a three-level four-leg NPC inverter. *IEEE Trans. Energy Convers.* **2017**, *32*, 23–35. [CrossRef]
14. Osman, I.; Xiao, D.; Alam, K.S.; Shakib, S.M.; Akter, M.P.; Rahman, M.F. Discrete Space Vector Modulation-Based Model Predictive Torque Control with No Suboptimization. *IEEE Trans. Ind. Electron.* **2020**, *67*, 8164–8174. [CrossRef]
15. Guo, L.; Jin, N.; Gan, C.; Xu, L.; Wang, Q. An improved model predictive control strategy to reduce common-mode voltage for two-level voltage source inverters considering dead-time effects. *IEEE Trans. Ind. Electron.* **2019**, *66*, 3561–3572. [CrossRef]
16. Alsofyani, I.M.; Lee, K.B. Improved Deadbeat FC-MPC Based on the Discrete Space Vector Modulation Method with Efficient Computation for a Grid-Connected Three-Level Inverter System. *Energies* **2019**, *12*, 3111. [CrossRef]
17. De Bosio, F.; de Souza Ribeiro, L.A.; Freijedo, F.D.; Pastorelli, M.; Guerrero, J.M. Effect of state feedback coupling and system delays on the transient performance of stand-alone VSI with LC output filter. *IEEE Trans. Ind. Electron.* **2016**, *63*, 4909–4918. [CrossRef]
18. Zhang, Y.; Qu, C. Model Predictive Direct Power Control of PWM Rectifiers Under Unbalanced Network Conditions. *IEEE Trans. Ind. Electron.* **2015**, *62*, 4011–4022. [CrossRef]
19. Alhasheem, M.; Blaabjerg, F.; Davari, P. Davari, Performance Assessment of Grid Forming Converters Using Different Finite Control Set Model Predictive Control (FCS-MPC) Algorithms. *Appl. Sci.* **2019**, *9*, 3513. [CrossRef]
20. Cortés, P.; Kazmierkowski, M.P.; Kennel, R.M.; Quevedo, D.E.; Rodríguez, J. Predictive control in power electronics and drives. *IEEE Trans. Ind. Electron.* **2008**, *55*, 4312–4324. [CrossRef]
21. Rivera, M. A new predictive control scheme for a VSI with reduced common mode voltage operating at fixed switching frequency. In Proceedings of the IEEE 5th International Conference on Power Engineering, Energy and Electrical Drives (POWERENG), Riga, Latvia, 11–13 May 2015; pp. 617–622. [CrossRef]
22. Pinto, J.O.; Bose, B.K.; Da Silva, L.B.; Kazmierkowski, M.P. A neural network based space vector PWM controller for voltage-fed inverter induction motor drive. *IEEE Trans. Ind. Electron.* **2000**, *36*, 1628–1636.
23. Chen, J.; Chen, Y.; Tong, L.; Peng, L.; Kang, Y. A Back propagation Neural Network-Based Explicit Model Predictive Control for DC–DC Converters with High Switching Frequency. *IEEE J. Emerg. Sel. Top. Power Electron.* **2020**, *8*, 2124–2142. [CrossRef]
24. Wang, D.; Yin, X.; Tang, S.; Zhang, C.; Shen, Z.J.; Wang, J.; Shuai, Z. A Deep Neural Network Based Predictive Control Strategy for High Frequency Multilevel Converters. In Proceedings of the IEEE Energy Conversion Congress and Exposition, Portland, OR, USA, 23–27 September 2018; pp. 2988–2992.
25. Mohamed, I.S.; Rovetta, S.; Do, T.D.; Dragicević, T.; Diab, A.A.Z. A Neural-Network-Based Model Predictive Control of Three-Phase Inverter with an Output LC Filter. *IEEE Access* **2019**, *7*, 124737–124749. [CrossRef]
26. Novak, M.; Dragicevic, T. Supervised imitation learning of finite set model predictive control systems for power electronics. *IEEE Trans. Ind. Electron.* **2020**, *68*, 1717–1723. [CrossRef]
27. Lucia, S.; Navarro, D.; Karg, B.; Sarnago, H.; Lucia, O. Deep Learning-based Model Predictive Control for Resonant Power Converters. *IEEE Trans. Ind. Inform.* **2020**, *17*, 409–420. [CrossRef]
28. Dragičević, T.; Novak, M. Weighting Factor Design in Model Predictive Control of Power Electronic Converters: An Artificial Neural Network Approach. *IEEE Trans. Ind. Electron.* **2018**, *66*, 2124–2142.
29. Bakeer, A.; Magdy, G.; Chub, A.; Bevrani, H. A sophisticated modeling approach for photovoltaic systems in load frequency control. *Int. J. Electr. Power Energy Syst.* **2022**, *134*, 107330. [CrossRef]
30. Awad, M.; Qasrawi, I. Enhanced RBF neural network model for time series prediction of solar cells panel depending on climate conditions (temperature and irradiance). *Neural Comput. Appl.* **2016**, *30*, 1757–1768. [CrossRef]